

We are IntechOpen, the world's leading publisher of Open Access books Built by scientists, for scientists

6,900

Open access books available

186,000

International authors and editors

200M

Downloads

Our authors are among the

154

Countries delivered to

TOP 1%

most cited scientists

12.2%

Contributors from top 500 universities



WEB OF SCIENCE™

Selection of our books indexed in the Book Citation Index
in Web of Science™ Core Collection (BKCI)

Interested in publishing with us?
Contact book.department@intechopen.com

Numbers displayed above are based on latest data collected.
For more information visit www.intechopen.com



Anomalous Rashba Effect of Bi Thin Film Studied by Spin-Resolved ARPES

Akari Takayama

Additional information is available at the end of the chapter

<http://dx.doi.org/10.5772/66278>

Abstract

The Rashba effect is a momentum-dependent splitting of spin bands in two-dimensional systems such as surface, interface and heterostructure. The effect is caused by broken space-inversion symmetry and spin-orbit coupling and allows to manipulate and generate the spin by the electric fields, that is, without the magnetic field. It means that the devices applied to the Rashba effect have many advantages. Bismuth is known as a promising candidate to investigate the surface Rashba effect, and the spin structure of Bi surface has also been intensively discussed. However, it is unclear to what extent the so far believed simple vortical spin structure is adequate. To understand the surface properties of the Rashba system is particularly important when utilizing the Rashba effect to the spintronic devices, since it is desirable to control the spin polarization when developing new types of devices. In this chapter, we report that the surface spin states of the Bi thin film exhibit unusual characteristics unlike the conventional Rashba splitting by using a spin- and angle-resolved photoemission spectroscopy measurement.

Keywords: Rashba effect, spin-resolved ARPES, thin film, bismuth

1. Introduction

As we know and use, spintronic devices to use a spin-polarized electrons have actualized. The magnetic storage technology uses giant magneto-resistance [1]. A more advanced approach is to control spin-polarized electrons without the aid of a ferromagnetism nor to apply the magnetic field [2]. Spin-orbit coupling (SOC) makes it possible to generate and manipulate spin-polarized electrons only by the electric field, since the electric field acts on a moving charge carrier as an effective magnetic field. Thus, it is regarded as an

essential ingredient for further development of next-generation spintronic devices such as the spin-field-effect transistor [3]. In nonmagnetic solids, the electronic states with opposite spin have the same energy (Kramers degeneracy) because of the time-reversal and the space-inversion symmetries (TRS and SIS). In the strong SOC environment with the broken space-inversion symmetry (typically at the surface or interface), the energy band splits in the momentum (k) space (Rashba effect [4]), leading to a spin helical structure of surface bands. This Rashba effect leads to the vortical spin structure of surface bands where the spin vector points parallel to the surface and perpendicular to the measured momentum. To be more specific, here we postulate the model of two-dimensional free electron gas at the surface. In the surface, as shown in **Figure 1a**, there is asymmetry of the potential in the direction perpendicular to the two-dimensional plane [$\nabla V = (0, 0, E_z)$]. When an electron moves with momentum (p), the $\nabla V \times p$ term acts as an effective magnetic field B_{eff} which is orthogonal to p ($=\hbar k$) and ∇V . As a result, the electron spin is quantized along the direction perpendicular to k in the surface plane. The energy of free electron gives the following,

$$E(k) = \frac{\hbar^2}{2m} k^2 \pm \alpha_R k \tag{1}$$

which is well known as the Rashba effect, where α_R is a so-called Rashba parameter. **Figure 1b** shows the band dispersion of this model. As described above, two-dimensional (2D) system with strong SOC has provided a useful platform for realizing novel quantum phenomena

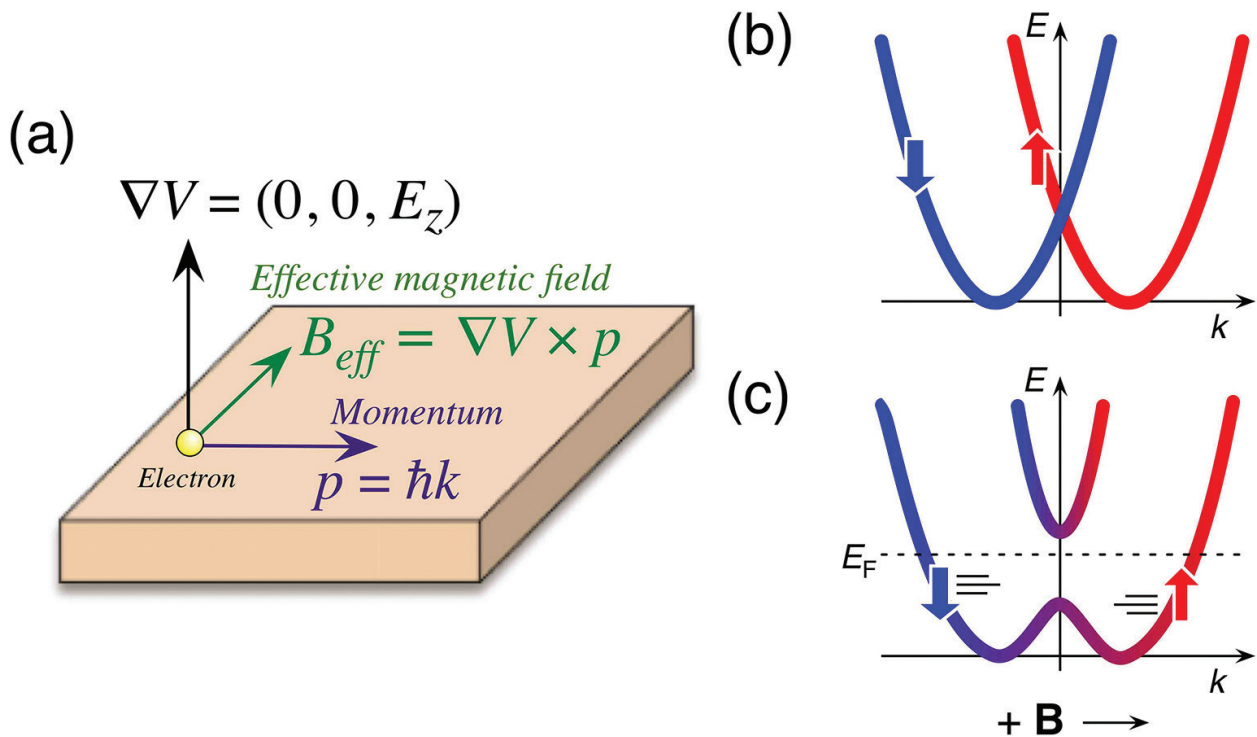


Figure 1. (a) Relationship between momentum (p) and surface potential (∇V) at surface. (b) Rashba-type spin-splitting band structure in 2D free electron gas model. (c) A band structure breaking the time-reversal symmetry by applying a magnetic field.

applicable to advanced spintronic devices [2, 5, 6]. To discuss and understand Rashba effect, spin- and angle-resolved photoemission spectroscopy (spin-resolved ARPES) is a powerful experimental technique, which can simultaneously determine all key quantum parameters of electrons in solids, that is, momentum, energy and spin. Furthermore, by high-resolution measurements, we will be able to discuss the spin-related physical phenomena not only qualitatively but also quantitatively, which would certainly lead to the deeper understanding of the condensed matter physics. Elucidation of the electron spin is very important to understand physical property in solid state and its surface as well as the possible applications to spintronic devices.

The first observation of the surface Rashba effect by ARPES is the Au(1 1 1) surface [7]. After that, various materials such as group-V semimetals and their alloy surfaces [8–16], as well as heavy-atom adsorbed semiconductor surfaces [17–22] and so on, are studied. Among them, the group-V semimetal bismuth (Bi) is a prime candidate to investigate the surface Rashba effect and many experiments and theoretical calculations studied in order to clarify the fundamental properties of the Rashba effect [8, 10–14]. However, in previous researches, although the band structure and Fermi surfaces of Bi distinctly show strong anisotropy, the spin structure of Bi was argued by assuming an isotropic two-circular Fermi-surface model like Au(1 1 1) [7, 20–22]. The reason is because the energy and momentum resolutions of the previous spin-resolved ARPES machine are insufficient. To understand whole aspect of the Rashba effect, it is necessary to clarify that the spin structure of Bi consists with the conventional Rashba model or not. Moreover, in the film, electronic states originating from the bulk Bi are quantized, and they are connected to the surface bands continuously. So it would be necessary to take into account the relationship between bulk and surface states. On the other hand, intensive attempts have been made to extend the investigations on 2D Rashba systems to quasi one-dimensional (1D) system like artificially grown nanowires and quantum wires, because of the merits in downsizing of devices. 1D Rashba effect in utilization of vicinal surfaces such as in Au chains on vicinal Si [23] and the vicinal Bi surface is also reported [24]. In such a case, breaking the TRS by applying magnetic field or adding magnetic impurities would create an energy gap at the Kramers point, and when the chemical potential is tuned to be located in the spin-orbit gap, the dissipation-less spin transport and the quantized conductance [25, 26] may be realized (**Figure 1c**). However, the Rashba effect in edge state is not known because the signal from the edge is extremely faint. To understand the proposed novel properties of a true 1D system, we may be able to apply them to advanced spintronic devices.

In this chapter, we introduce the electronic structure of Bi thin film to elucidate the details of the Rashba effect by utilizing the high-resolution spin-resolved ARPES spectrometer equipped with a highly efficient mini-Mott detector. We show three novel Rashba effects of Bi thin film: (i) anisotropic Rashba effect from momentum-dependent measurement [27], (ii) the interface Rashba effect between metal-semiconductor from thickness-dependent [28] and (iii) 1D Rashba effect of edge state [29]. The present finding provides a useful platform to study the Rashba effect and at the same time opens a pathway to utilize the novel properties to advanced spintronic devices.

2. Experimental technique and sample fabrication

2.1. Spin- and angle-resolved photoemission spectromete

Figure 2 shows a schematic diagram of the ultra-high-resolution spin-resolved ARPES spectrometer with a highly efficient mini-Mott detector [30]. This spectrometer consists of mainly four parts: (i) a photoemission measurement system including a hemispherical electron energy analyzer and an ultra-high-vacuum measurement chamber, (ii) a spin-detection system based on a mini-Mott detector, (iii) an intense xenon/helium plasma discharge lamp and (iv) a surface chamber to prepare the thin-film samples. We explain the detail of each part. We have improved a MBS-A1 electron energy analyzer to achieve both spin-resolved and regular (non-spin-resolved) ARPES measurement. The spectrometer has two detectors: one is a multichannel plate for ARPES measurement, and the other is mini-Mott detector for spin-resolved ARPES. To determine the three-dimensional spin polarization, an electron deflector has been placed between the analyzer and the Mott detector. The Mott detector observes the spin polarization of essentially two independent axes by using four channeltrons, enabling us to determine the in-plane and out-of-plane spin component. The scattering efficiency of the Mott detector is as high as 2.3×10^{-2} . The optical system consists of helium (He) and xenon (Xe) plasma discharge lamps and a monochromator with the gratings, in which we can select

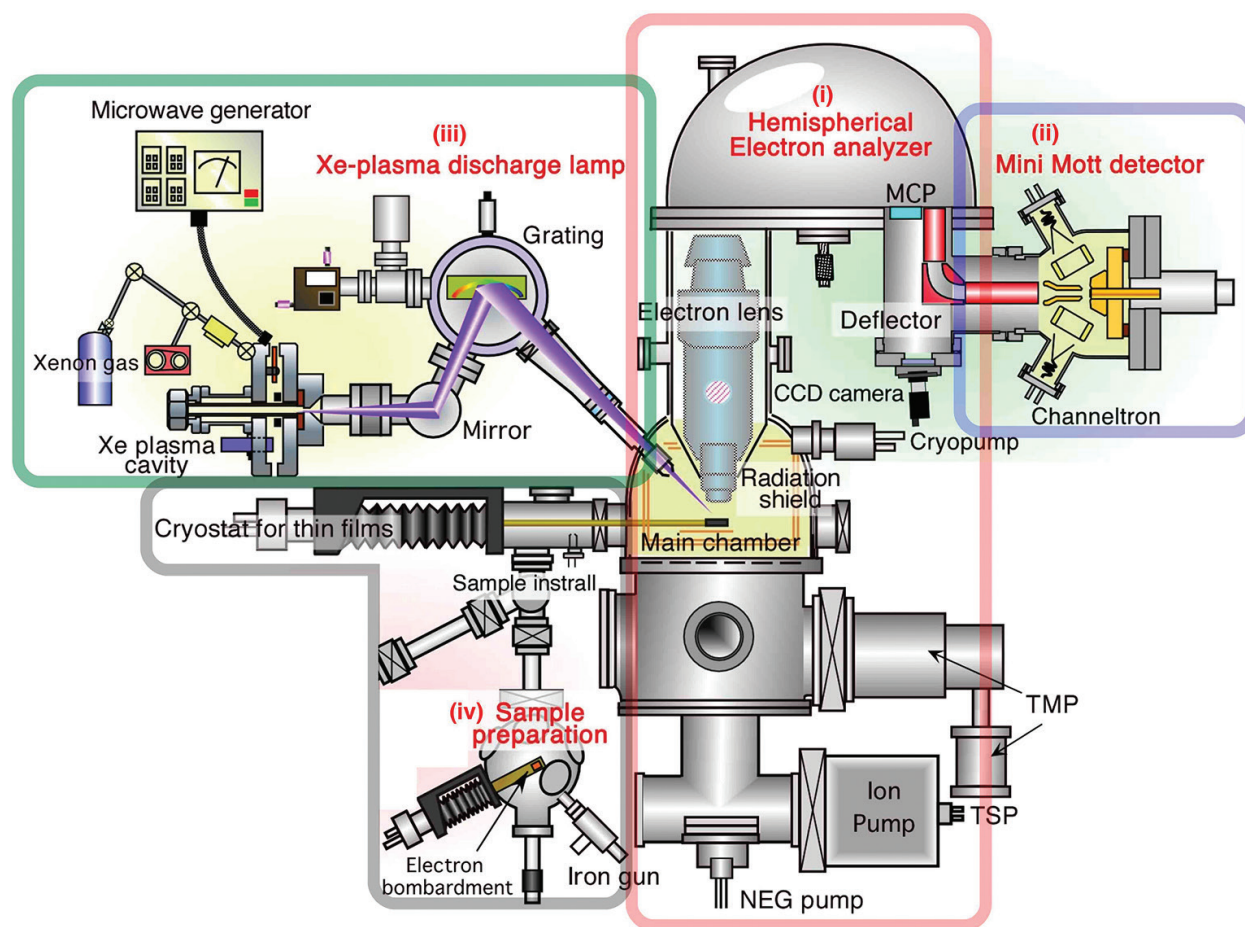


Figure 2. Schematic view of high-resolution spin-resolved photoemission spectrometer.

photon energy if necessary. In this study, we used one of the Xe I lines ($h\nu = 8.437$ eV) to excite photoelectrons. In order to fabricate high-quality samples, a surface chamber has been constructed and is connected to the spin-resolved ARPRS spectrometer. The spectrometer achieves the energy resolutions of 0.9 and 8 meV for non-spin-resolved and spin-resolved modes, respectively. **Figure 3** shows a schematic view of the surface chamber. A surface chamber contains heating systems for a semiconductor sample, a few kinds of dispensers, a quartz crystal microbalance and a low-energy electron diffraction (LEED) system for checking the quality of the sample surface. The vacuum of the surface chamber is basically kept 1×10^{-10} Torr to prepare a high-quality sample surface. It allows the in situ preparation of the sample and its transfer to the spin-resolved spectrometer. It is particularly useful for elucidating the electronic states of the samples containing a clean well-ordered surfaces required for the accurate ARPES measurements. Thus, we can prepare the Bi thin-film samples by the evaporation of Bi on semiconducting substrate. We expect that the performance of the spectrometer is demonstrated by the observation of a clear Rashba splitting of the surface states in Bi. The energy and momentum resolutions for the regular (spin-integrated) ARPES were 5–20 meV and 0.3° , and for spin-resolved ARPES measurements were 40 meV and 3° , respectively. The Sherman function value was set at 0.07. The measurement temperature was 300 and 30 K.

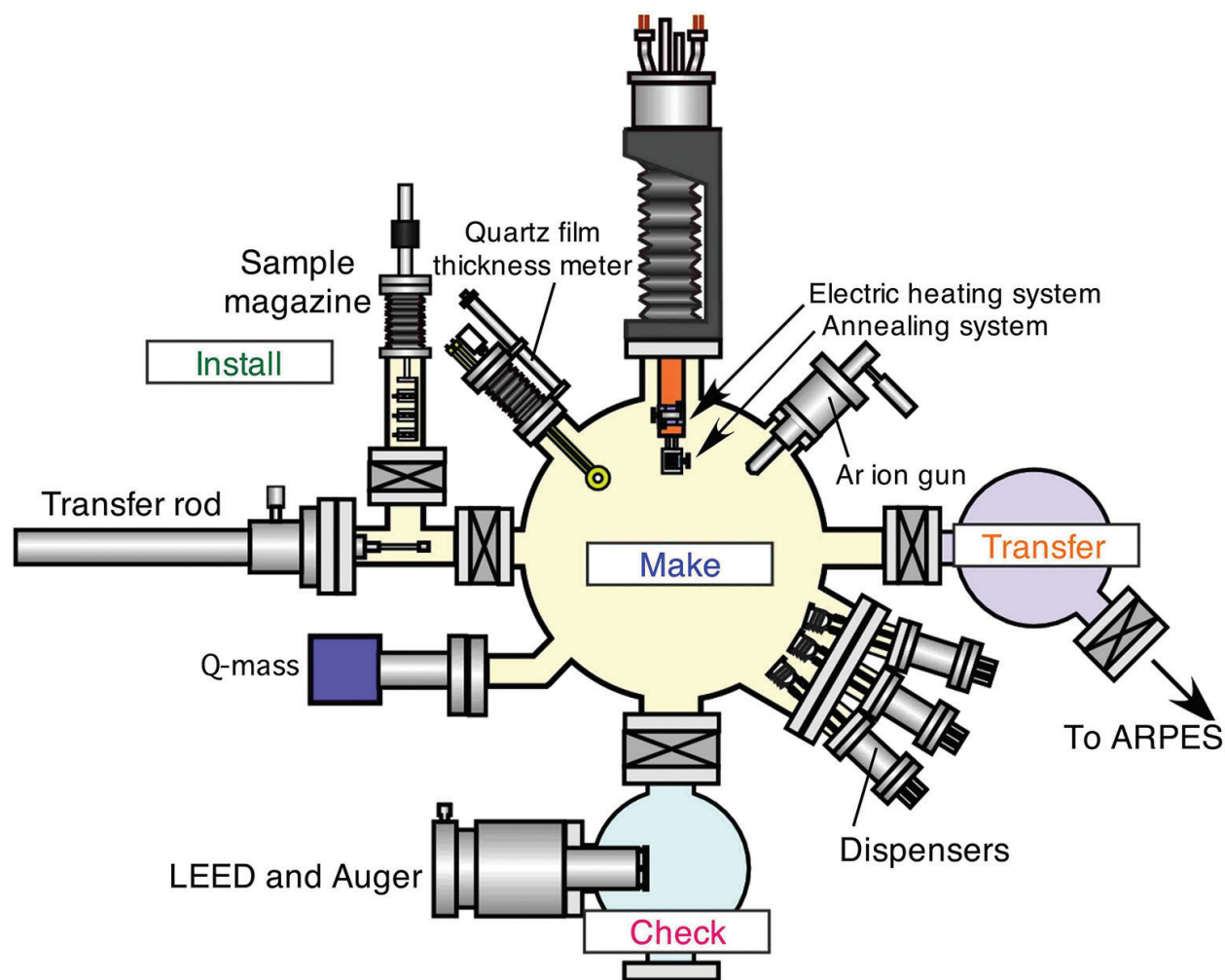


Figure 3. Schematic view of the sample preparation chamber.

2.2. Sample fabrication

To get a high-quality Bi(1 1 1) thin film, we prepare a clean surface of the Si(1 1 1) substrate. We use a commercially available Si wafer (n-type, As-doped: 0.001–0.005 Ω cm, Sb-doped: 0.01–0.02 Ω cm), and the surface of Si forms native SiO₂ in the air. So we must remove it by electrical heating in high vacuum. **Figure 4** displays the design of a holder for the electrical heating system (**Figure 4**). The holder is made of molybdenum, and a main holder is insulated from a subholder by the alumina. We can control a current and temperature with 5 mA and 1°C, respectively. The sample size is 13 × 3 mm, and we have selected four different kinds of crystal orientations on the basis of orientation flat as shown in **Figure 5**. The sample geometry has been confirmed by the brightness symmetry of the LEED spots. The most stable structure of the Si(1 1 1) surface is the 7 × 7 reconstructed surface, as shown in **Figure 6a** [31, 32]. Now, we describe the method to pre-

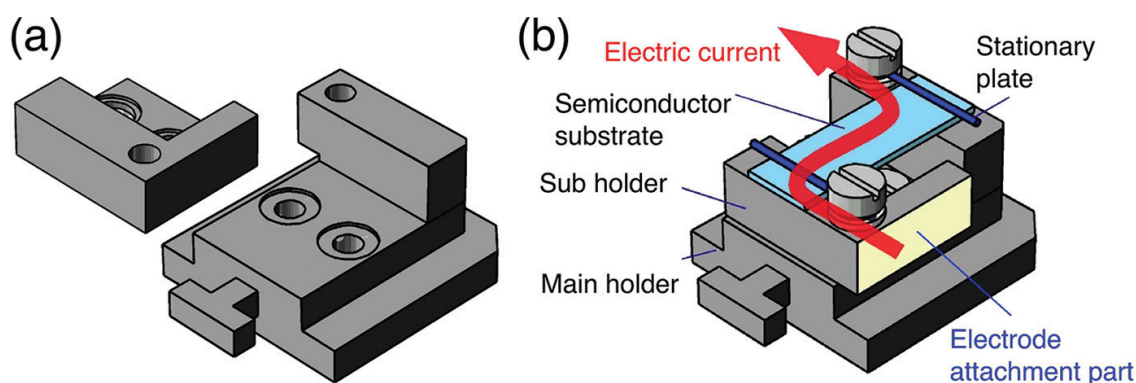


Figure 4. (a) A main and subparts of sample holder. (b) A constructed holder.

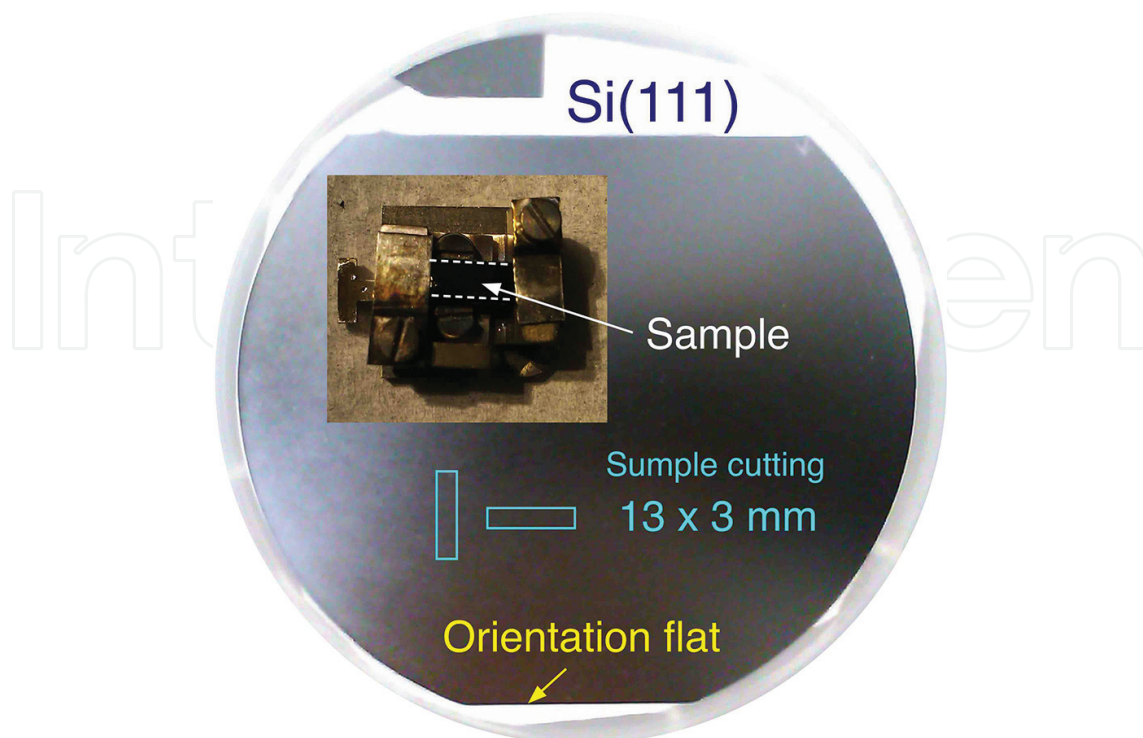


Figure 5. Cutting the sample from the Si(1 1 1) wafer. Inset shows the picture of a sample holder compared to the sample size. The geometry of the sample was determined by the direction of “orientation flat.”

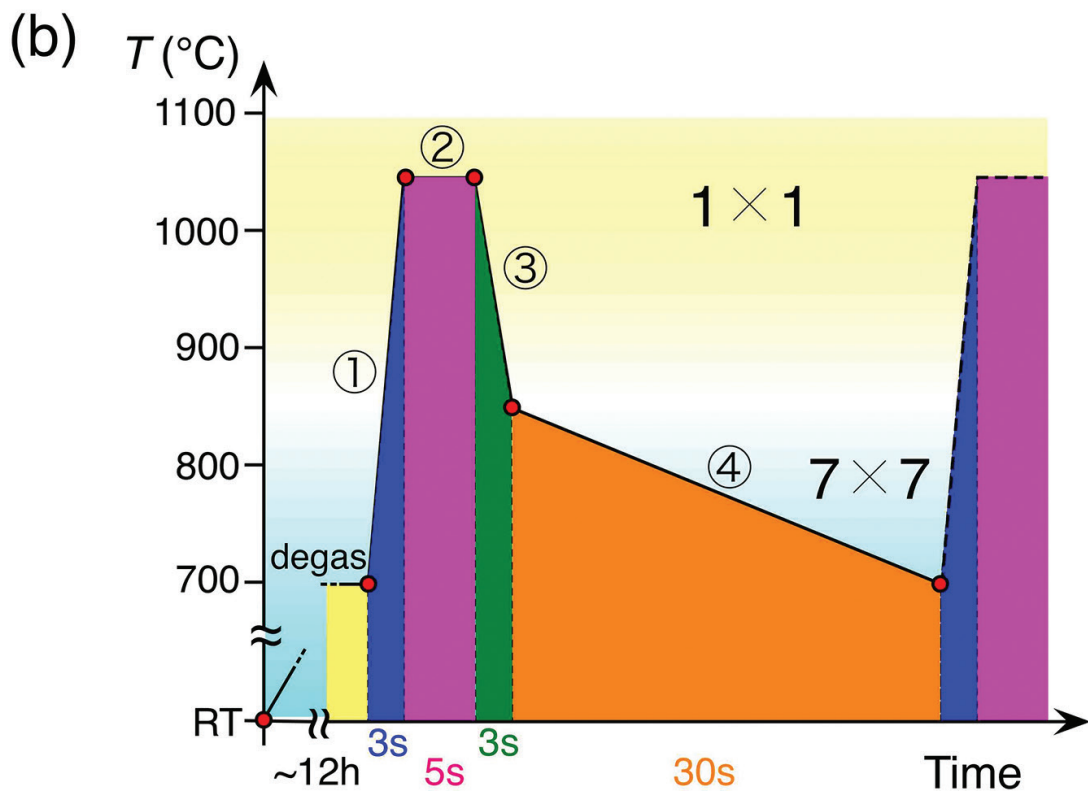
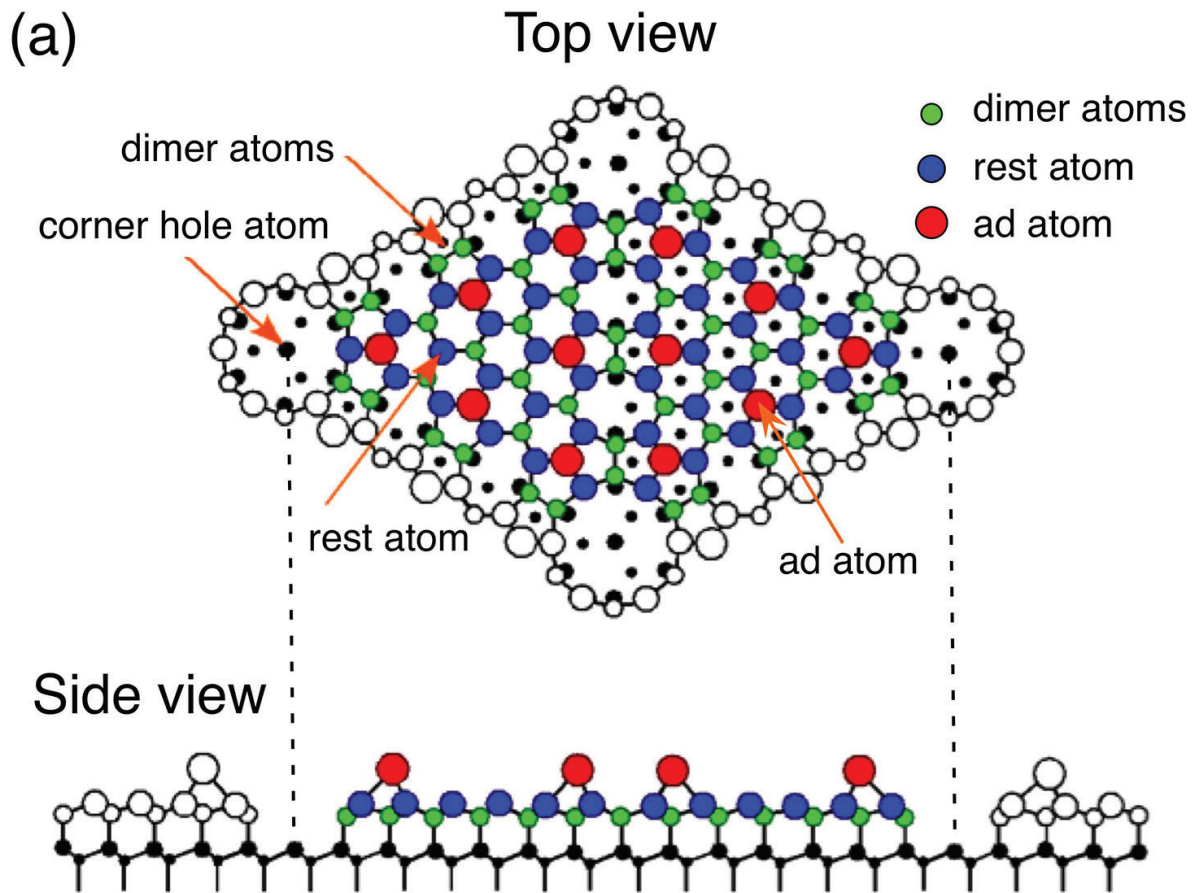


Figure 6. (a) Atomic-structure model (Das model) of Si(111)-7×7. (b) Detailed annealing process to prepare the Si(111)-7×7 clean surface.

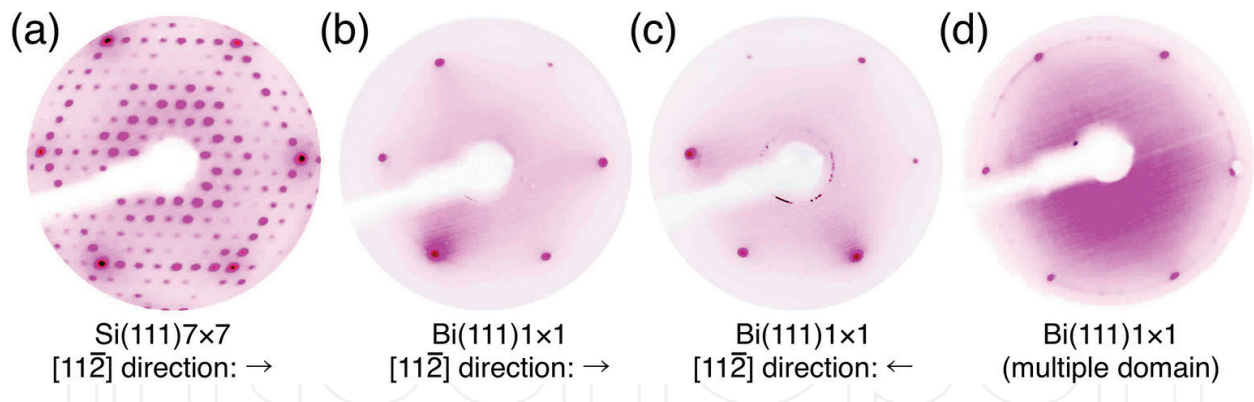


Figure 7. Comparison of the LEED pattern. (a) Si(1 1 1)-7 \times 7. (b) and (c) Bi(1 1 1)-1 \times 1. These two samples have a different cutting directions from Si wafer [sample direction in (c) is rotated in 180° from (b)]. (d) A multiple-domain sample of Bi(1 1 1)-1 \times 1.

pare a Si(1 1 1)-7 \times 7 reconstructed surface. First, the Si wafers were outgassed for more than 12 h below 750°C. After the outgassing enough, we have carried out flash annealing. **Figure 6b** shows a flash-annealing process to get a Si(1 1 1)-7 \times 7 reconstructed surface; sample was (i) heated at 750°C to 1050–1200°C for a few seconds, (ii) keep temperature to maximum for 5 s, (iii) cooled down to 850°C for a few seconds and (iv) cooled to 750°C in 30 s [33]. We have repeated this cycle, and all of the above processes should be performed under the ultra-high vacuum of $\sim 1 \times 10^{-10}$ Torr. As shown in **Figure 7a**, we have obtained the LEED pattern of the well-ordered 7 \times 7 surface.

Next, Bi atoms are evaporated on Si substrate, which is called as a molecular beam epitaxy (MBE). Bi atoms are deposited at room temperature on Si(1 1 1)-7 \times 7 reconstructed surface. Then, the Bi thin film was annealed at 150°C. The deposition rate is estimated by the quartz oscillator thickness monitor, and the film thickness was controlled by varying the deposition time with keeping the constant deposition rate. We can also estimate the film thickness from the energy position of the quantum well states (QWSs) in the ARPES spectra [28]. It is noted that 1 bilayer (BL) Bi is defined as 1.14×10^{15} atoms/cm², and the thickness is 0.39 nm [13]. In this study, we prepared several thickness sample (8–40 BL). After the deposition of Bi atoms, the LEED pattern shows the 1 \times 1 surface structure as shown in **Figure 7b** and **c**, and the intensity of the LEED spot has threefold symmetry. When the sample has a multi-domain structure, the LEED pattern shows circular features surrounding the 1 \times 1 spots (**Figure 7d**). We could repeatedly use one Si substrate by a flashing. Here we describe a structure of Bi thin film on Si substrate. Details of the thin-film growth process are shown in **Figure 8a**, which is reported in previous works such as STM and LEED [34]. Although the lattice constant of Bi (4.538 Å) is very different from Si (5.43 Å), it is possible to fabricate the Bi/Si thin film due to the existence of disordered layer called “wetting layer” between Bi and Si substrate. As shown in **Figure 8b**, the structural transition from {0 1 2} direction to (1 1 1) direction more than 8.4 ML suddenly takes place upon Bi deposition.

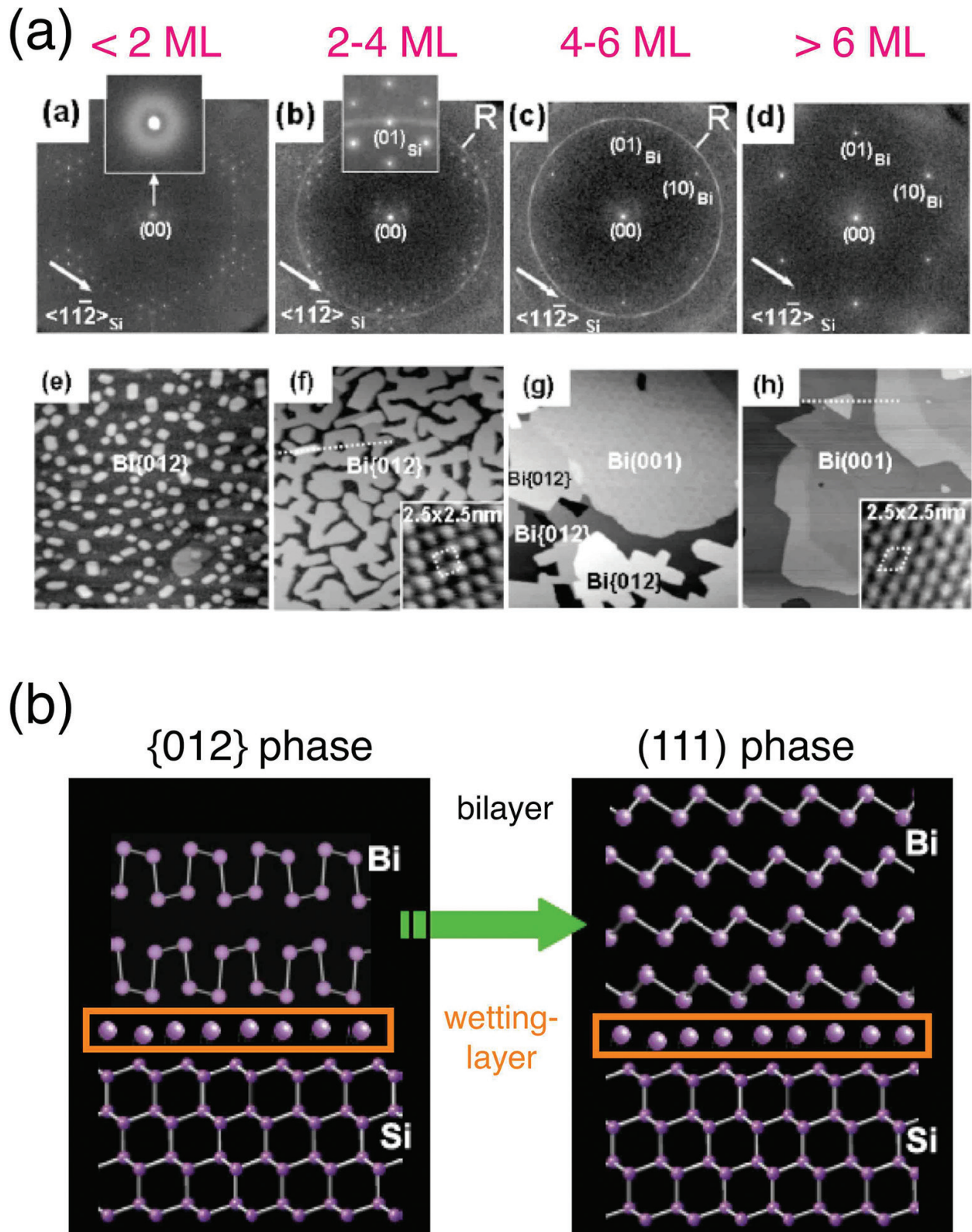


Figure 8. (a) Thickness dependence of spot-profile-analyzing-LEED pattern (top) and STM image (bottom) [34]. (b) Schematic illustration of the transformed structure in growth process of Bi thin film [34].

3. Results and discussion

3.1. Anisotropic Rashba effect of Bi thin film

At first, we have performed normal (non-spin-resolved) ARPES measurement of the Bi thin film in order to check the sample quality and geometry, since even a subtle misalignment of the sample orientation would cause a significant error in determining the spin polarization. **Figure 9a** and **b** shows the band dispersion along the $\bar{\Gamma}\bar{M}$ line and Fermi surface of Bi/Si(1 1 1). Areas with hatched lines in **Figure 9a** are bulk band projection. We distinctly see that several bands cross E_F and three kinds Fermi surfaces exist; a hexagonal Fermi surface centered at the $\bar{\Gamma}$ point (S_1), surrounding elongated pockets (S_2) and the ellipsoidal pocket (S_3) near the \bar{M} point. Judged from the band dispersion in **Figure 9a**, the S_1 and S_3 are attributed to the electron pockets, while the S_2 to a hole pocket, all of which arise from the spin-split surface states [8, 10–14].

This section focuses on the spin structure of the S_2 band. In a conventional 2D Rashba model, the in-plane spin has a vortical structure and isotropic magnitude as denoted by black arrows in **Figure 10a**. In **Figure 10b** and **e**, we display the near- E_F spin-resolved energy distribution curves (EDCs) for the in-plane (y/x) and out-of-plane (z) spin components measured in various k regions, A–J as shown in **Figure 10a**. As displayed in **Figure 10b** and **e**, the spin-resolved

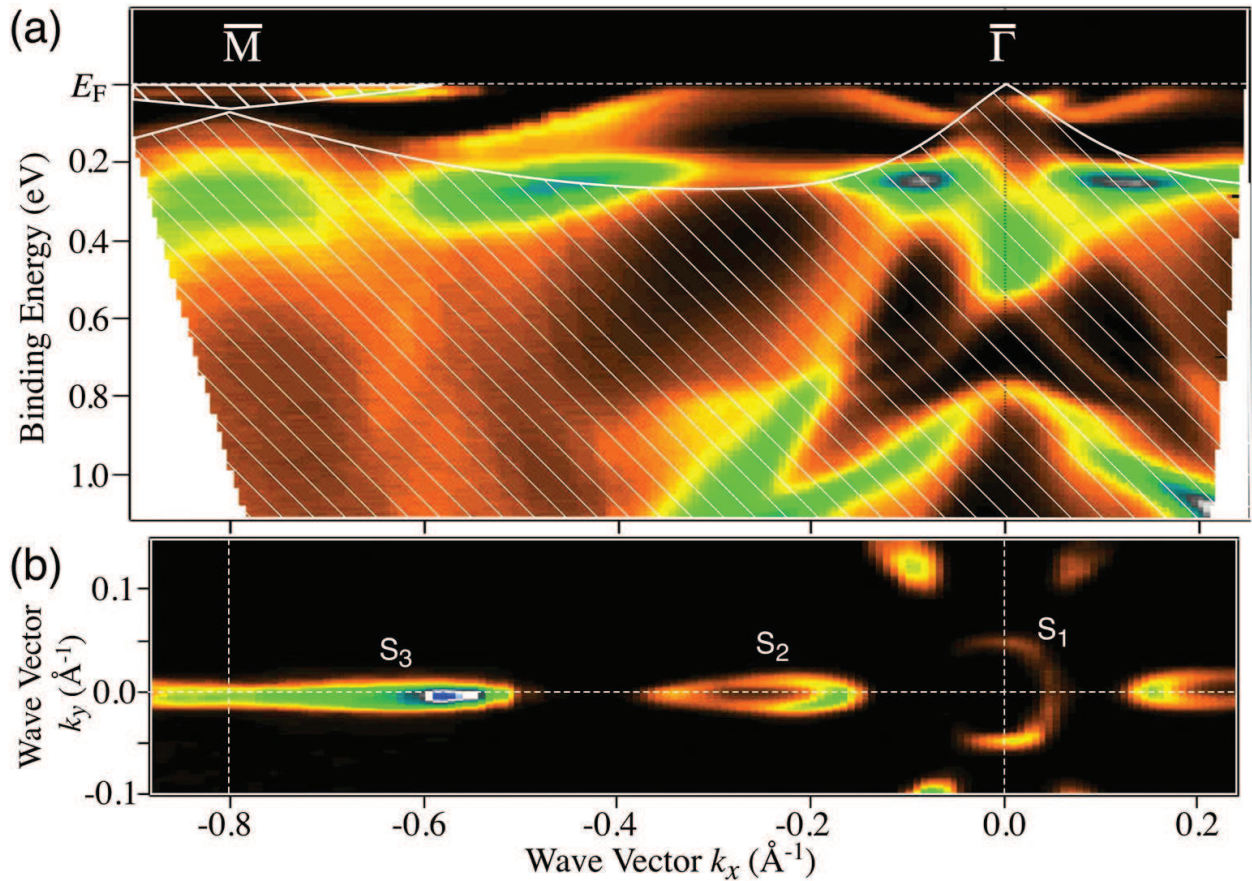


Figure 9. (a) Band dispersion of the ARPES spectra of Bi/Si(1 1 1) along the $\bar{\Gamma}\bar{M}$ line at $T = 30$ K. Shaded areas indicate the bulk band projection. (b) 2D ARPES intensity plot at E_F as a function of k_x and k_y around the $\bar{\Gamma}\bar{M}$ line.

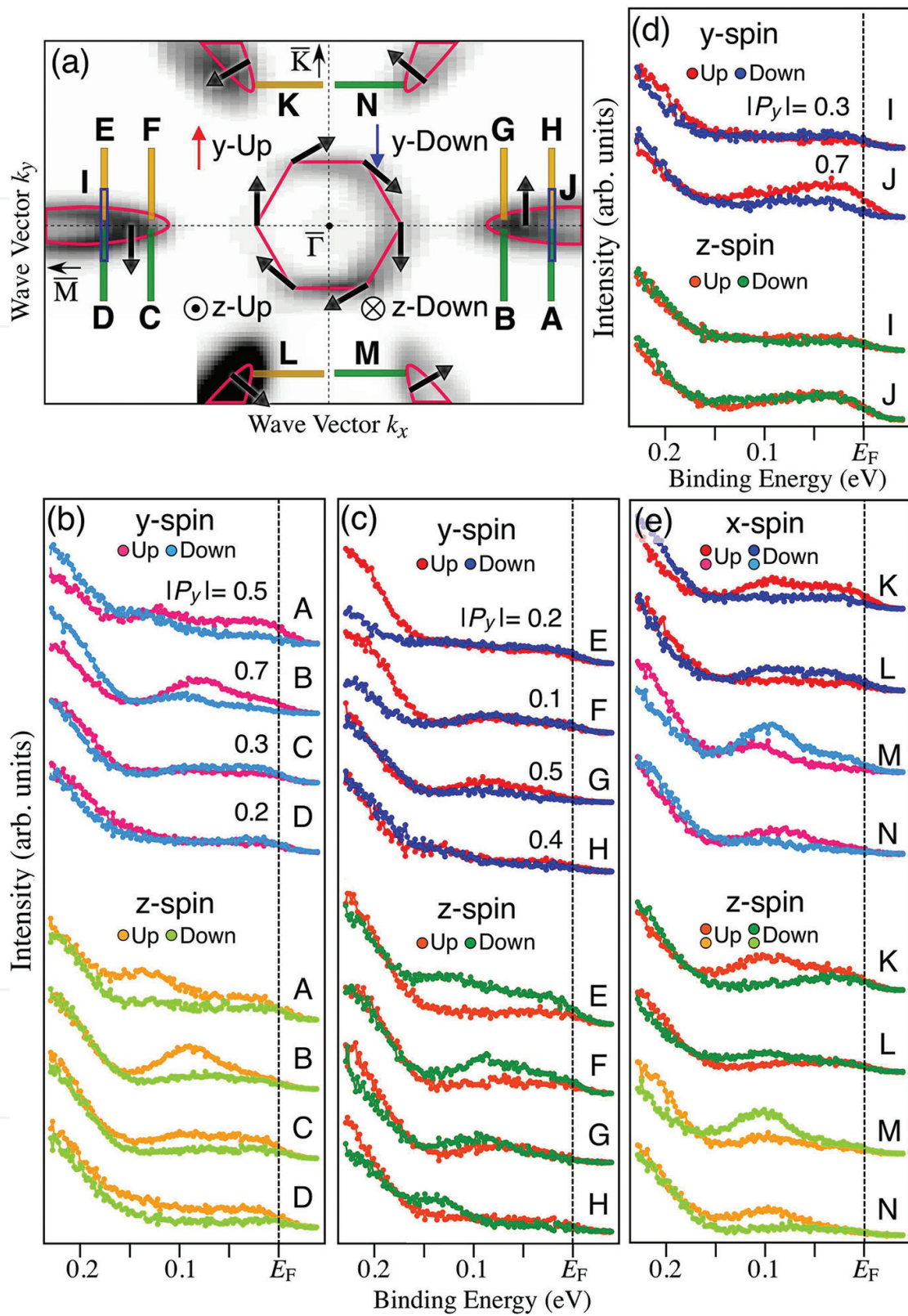


Figure 10. (a) Fermi surface of Bi/Si(111) around the $\bar{\Gamma}$ point. Red lines are guides for the Fermi surface of the surface bands. Lines A–N represent the k region where the spin-resolved EDCs in (b) and (e) were obtained. Expected spin configuration from the normal Rashba spin-orbit coupling is indicated by black arrows. Spin-resolved EDCs in regions (b) A–D, (c) E–H, (d) I, J and (e) K–N, respectively.

EDC mainly consists of two components: a slope-like feature, which rapidly increases its intensity at the binding energy (E_B) higher than 0.15 eV corresponding to the tail of the QWS, and a weaker broad feature at E_F -0.1 eV assigned as the S_2 band.

First, we take a closer look at the spin polarization in regions A–D. In regions A and B, as seen in **Figure 10b**, the in-plane spin polarization of the S_2 band is dominated by the up spin. On the other hand, the down spin is barely superior in regions C and D. It means that the in-plane spin structure is qualitatively consistent with the Rashba picture [13–14]. However, it seems that the spin polarization is markedly suppressed in C and D. In fact, the magnitude of the spin polarization along the y direction $|P_y|$ is 0.5–0.7 in regions A and B, while it is 0.2–0.3 in regions C and D. This is unexpected since $|P_y|$ should keep the same value across the $\bar{\Gamma}$ point in the normal Rashba picture. Then, we focus on the out-of-plane (z) spin component. We immediately notice that there exists a sizable up-spin polarization, while theoretically predicted out-of-plane spin polarization for simple isotropic Rashba system is zero. More surprisingly, the magnitude of the z -axis spin polarization $|P_z|$ (0.4–0.7) is as large as that of $|P_y|$.

We have also observed a finite in-plane and out-of-plane spin polarization in regions E–H. As shown in **Figure 10c**, the estimated maximum $|P_y|$ of the S_2 band in regions E and F (0.1–0.2) is much smaller than that in regions G and H (0.4–0.5), and it is similar to the result of regions A–D. But then, the down-spin component dominates for out-of-plane spin polarization in regions E–H. This result suggests that P_z has opposite spin direction across the $\bar{\Gamma}$ – \bar{M} line: the up-spin component is superior in the negative k_y (regions A–D), while the down-spin component is superior in the positive k_y (regions E–H).

The data in regions I and J are also the same trend as shown in **Figure 10d**. The difference in $|P_y|$ across the $\bar{\Gamma}$ point is also recognized by comparing the EDCs between regions I and J. In addition, the value of $|P_z|$ (~zero) is a good agreement in regions I and J where the up- and down-spin components almost overlap with each other because of the cancellation of two opposite spins. To see if a similar trend is observed along another high-symmetry line $\bar{\Gamma}$ – \bar{K} , we demonstrate in **Figure 10e** the spin-resolved EDCs measured in regions K–N. It is apparent that the sign of P_z (also P_x) in region K (L) is the same as that in the region N (M), indicating that P_z (P_x) does not switch the sign across the $\bar{\Gamma}$ – \bar{K} line.

Figure 11 shows a schematical view of the spin polarization vectors of the S_2 band from **Figure 10**. We symmetrized the data by taking into account the threefold crystal symmetry due to the presence of a second bismuth layer. The in-plane spin component has a vortical structure, but the magnitude of the spin polarization is perpendicular to k , called here P_θ . P_z has a large component and switches the sign by every 60° step. These features would lead to the periodic oscillation of P_θ and P_z , unlike the general Rashba SOC where $P_\theta = \text{const}$ and $P_z = 0$. Now, we discuss the origin of anomalous Rashba effect of Bi thin film. In the conventional Rashba effect, the in-plane spin polarization of S_2 is symmetry with respect to the $\bar{\Gamma}$ point. In this study, the TRS is not broken by some magnetic impurities because the Bi and Si are nonmagnetic materials. Another possibility of causing the broken TRS is the local surface conditions or the final-state effect [35, 36]. However, this possibility might be also unlikely by the reproducibility of data and comparing with previous studies. Here it is noted that the LEED pattern of Bi/Si(1 1 1) in **Figure 7** shows the threefold symmetry due to the bilayer-Bi

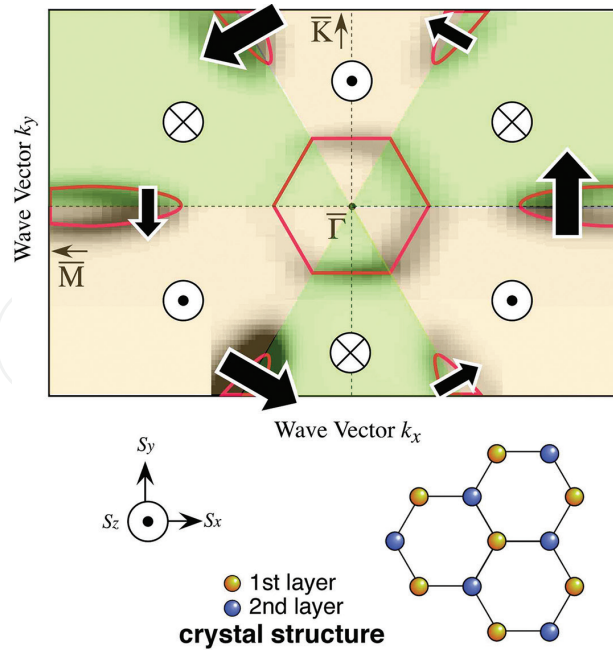


Figure 11. Schematic view of the spin structure of the S_2 hole pocket in Bi/Si(1 1 1). Size of arrows roughly scales with the observed spin polarization. Data are folded by taking into account the threefold symmetric variation of the bilayer-crystal structure.

crystal structure, and we conjecture that the origin of the in-plane spin asymmetry would be related to the crystal symmetry at present. Next, we discuss the out-of-plane spin polarization. Unlike in-plane spin polarization, the threefold symmetry in the out-of-plane spin component is reported, and sign-switching behavior is in good agreement with the previous studies in Bi/Ag(1 1 1) and Bi_{1-x}Sb_x [15, 37]. The spin structure of Bi surface state is also similar to the spin-resolved ARPES experiments on the hexagonally warped Dirac-cone Fermi surface of the topological insulator as well as the prediction of the $k\hat{A}\cdot p$ theory [38, 39]. On the other hand, the absolute value of the out-of-plane spin polarization obtained by our experiment is 40–70%, while the theoretical value of previous studies is a few percent. In order to clarify the spin structure of Bi Rashba effect, we need to evolve theoretical and experimental studies.

3.2. Rashba effect at interface of a Bi Thin film on Si(1 1 1)

In this section, we focus on the spin structure around the \bar{M} point of the Bi/Si(1 1 1) thin film. As shown in **Figure 12a**, the band dispersion of the QWSs dramatically alters around the \bar{M} point as a function of the film thickness d , and we prepared five different thickness film for $d = 8, 10, 15, 20$ and 40 BL. All of the samples, the bottom energy of an electron-like dispersion is located at ~ 30 meV below E_F . This band is well separated from the hole-like band at higher E_B arising from the QWSs that originate from the confinement of the wave function in the direction perpendicular to the surface (z direction). There is no evidence for the Kramers degeneracy of the S_3 band or the QWSs at the \bar{M} point ($k_y = 0$). The absence of the Kramers degeneracy at the \bar{M} point has also been observed in the previous research of the Bi, and it is explained by the

hybridization of the surface states and the QWS [9, 12]. As clearly visible, we identify the QWSs at $E_B = 0.1\text{--}0.25$ eV for $d = 40$ BL. Upon decreasing d , the top of the highest QWS shifts downward, and the energy separation of each QWS becomes wider, enabling us to unambiguously identify the overall energy dispersion of the individual QWS in the band dispersion plots.

In conventional Rashba picture, the in-plane spin polarization of the S_3 band is dominated by the up spin independently of a thickness at the cut 1 shown in **Figure 12b**. **Figure 12c** shows the spin-resolved EDCs and spin polarization of P_y for various d values of 8–40 BL. All of the spin-resolved EDCs consist of the tail of the QWSs at $E_B > 0.1$ eV and the S_3 electron band at ~ 50 meV. As seen in **Figure 12c**, the in-plane spin-resolved EDCs of the S_3 band for 10–40 BL are dominated by the up spin, and this indicates that the in-plane spin direction is qualitatively consistent with the normal Rashba picture. However, our result clearly demonstrates that the observed P_y value strongly depends on d . The obtained P_y value at $d = 40$ BL has a maximum at ~ 0.7 , then gradually reduces at $d = 15$ BL ($P_y \sim 0.3$) and finally reaches ~ 0 at $d = 8$ BL. It is noted that the much smaller spin polarization in the above- E_F region for $d = 15$ BL as compared to that for $d = 40$ BL might be due to much weaker peak weight in the original EDC and an intrinsic suppression of the spin polarization, which would lead to a relative enhancement of the background weight and less statistical reliability of the states above E_F .

We discuss the physical mechanism behind the unusual thickness dependence of P . The coupling between the Bi film and the Si(1 1 1) substrate is fairly weak due to the presence of a disordered wetting layer at the interface, suggesting that the Bi film is nearly freestanding [34]. Namely, the Bi/Si interface is also broken SIS, and it can be thought of as another (bottom) surface as with vacuum-side (top) surface. These Rashba states of top and bottom surface should have opposite spin directions as illustrated in **Figure 13**. In case of bulk Bi, which is thick enough, the top and bottom Rashba states do not interfere with each other. On reducing

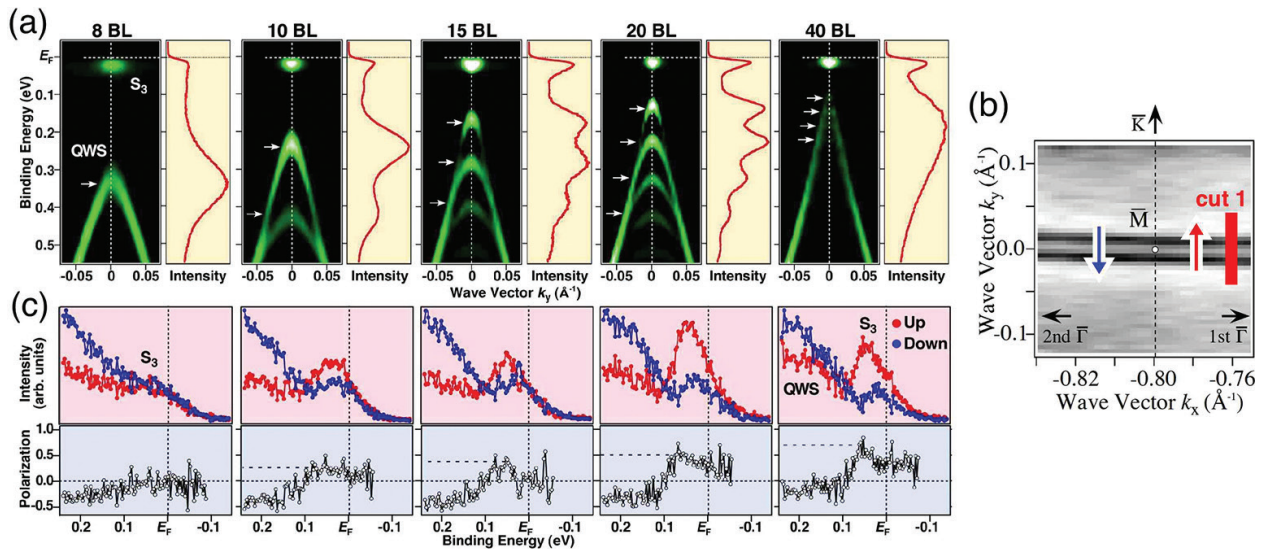


Figure 12. (a) Thickness dependence of the band dispersion near E_F along the $\overline{K}\overline{M}\overline{K}$ line, obtained by taking the second derivative of the EDCs at 30 K. EDC at the \overline{M} point is also shown for each thickness. (b) The Fermi surface around the \overline{M} point. Blue and red arrows indicate expected spin configuration of the normal Rashba effect. (c) Corresponding spin-resolved EDCs and their spin polarizations for cut 1 in (b).

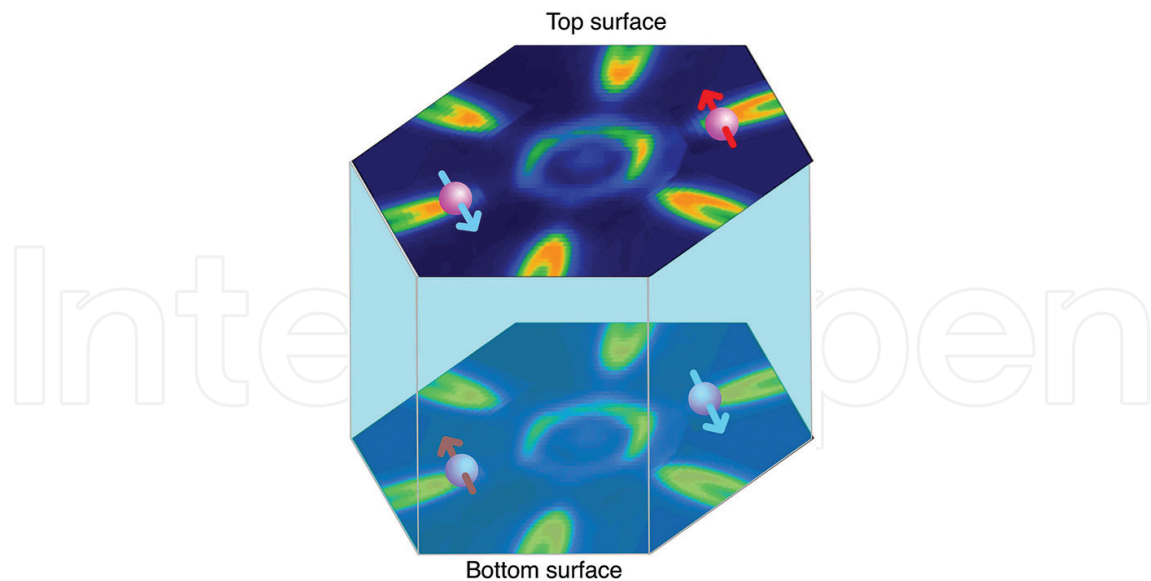


Figure 13. Schematic view of the spin vectors for the Fermi surface at the top and bottom surfaces.

thickness, the wave functions of the two Rashba states overlap and hybridize, which means that the up- and down-spin states merge and the P observed by spin-resolved ARPES would become small. This picture is a very simple model but explains in a nice way the thickness dependence of P . We also found that the decay length of the surface-state wave function is around at least 20 BL (~ 80 Å) since the reduction in experimental P is already started in 20 BL (**Figure 12**). A thin film of Bi_2Se_3 topological insulator also exhibits a similar decay length, as inferred from the experimental fact that the hybridization gap starts to open at six quintuple layers (~ 60 Å) [40]. Our result also suggests that the Rashba effect of Bi/Si interface is useful for the spintronic devices because the interface is generally more stable than the surface.

3.3. 1D edge state with Rashba effect in Bi thin film

As observed by the atomic force microscopy of our Bi thin film (**Figure 14**), triangular-shaped Bi BL islands with typically ~ 0.1 μm edge length are formed on the top surface of the Bi thin film as reported previously [34], and the edge of each island is perpendicular to the $\bar{\Gamma}\bar{M}$ direction considering sample geometry; namely, the edge runs along the $\bar{\Gamma}\bar{K}$ direction in the k space. According to previous experimental and theoretical studies, there are no bulk and surface states near the \bar{K} point, and we might observe some electronic state if edge state exists along the $\bar{\Gamma}\bar{K}$ line.

We demonstrate the band dispersion of Bi thin film along the $\bar{\Gamma}\bar{K}$ line for $d=15$ BL in **Figure 15**. With a careful look at the region between $\bar{\Gamma}\bar{K}$ line (yellow rectangle in **Figure 15a**), one finds unexpected faint intensity displaying a finite energy dispersion, as better illustrated with enhanced color contrast in the inset. To establish the energy dispersion of this unexpected feature, we have measured the ARPES data along several cuts in the surface Brillouin zone (**Figure 15b**). A careful band searching with the enhanced intensity scale (**Figure 15c**) shows the band dispersion with a characteristic x -shape along cuts 1–3. The intersection of

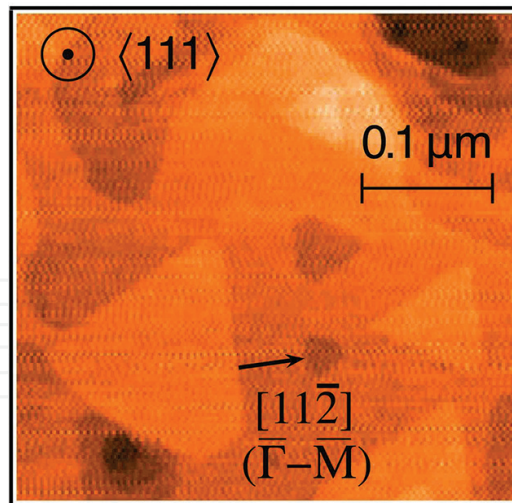


Figure 14. The atomic force microscopy image of a Bi thin film ($d = 15$ BL) at $T = 300$ K.

the x -shaped band is at $k_y \sim 0.7 \text{ \AA}^{-1}$ not at the high-symmetry points of the surface and bulk Brillouin zone. Intriguingly, this band is robust against the change in the k_x location of cut (cuts 1–3). This demonstrates that the x -shaped dispersion has a 1D character along the k_y direction. Indeed, the observed band structure along cut 4 (perpendicular to cuts 1–3) shows no obvious dispersion, confirming the 1D nature. To experimentally clarify the spin-split nature of the edge band, we have performed a spin-resolved ARPES experiment. As shown in **Figure 15d** which plots the spin-resolved EDCs at a representative k_y point (marked by a pink line in **Figure 15c**), we clearly find a difference between the up- and down-spin spectra in both the in-plane and out-of-plane components.

As for the origin of the unexpected 1D state, we have taken into account various possibilities such as the mixture of domains with different film thickness, surface reconstruction, slight isolation of the topmost Bi bilayer and surface stacking faults. A most natural and convincing explanation is that it originates from the edge states of Bi bilayer. To further strengthen our conclusion, we have carried out first-principles electronic band structure calculations for a specific crystal structure (**Figure 16**). Electronic band structure calculations were carried out by means of a first-principles density functional theory approach with the all-electron full-potential linearized augmented-plane-wave method in the scalar relativistic scheme. The spin-orbit coupling was included as the second variation in the self-consistent-field iterations. Thin-film systems were simulated by adopting periodic slab models with sufficiently thick vacuum layer. In this model, Bi atoms in 1D allay are removed from the topmost Bi 1BL (**Figure 16a**) so as to reproduce the infinitely long edge structure along the y direction. Assumption of such an idealized model crystal is turned out to be sufficient for reasonably simulating the edge band structure. As shown in **Figure 16c**, the Brillouin zone for this model crystal structure has a rectangular shape. The vertical length of Brillouin zone is the same as the $\bar{\Gamma}-\bar{M}-\bar{M}$ interval since the size of unit cell along y -axis is the same for the edge structure and the Bi thin film. On the other hand, the horizontal Brillouin zone length has no important physical role because the unit-cell length for x -axis was simply chosen for the sake of calculations. Thus,

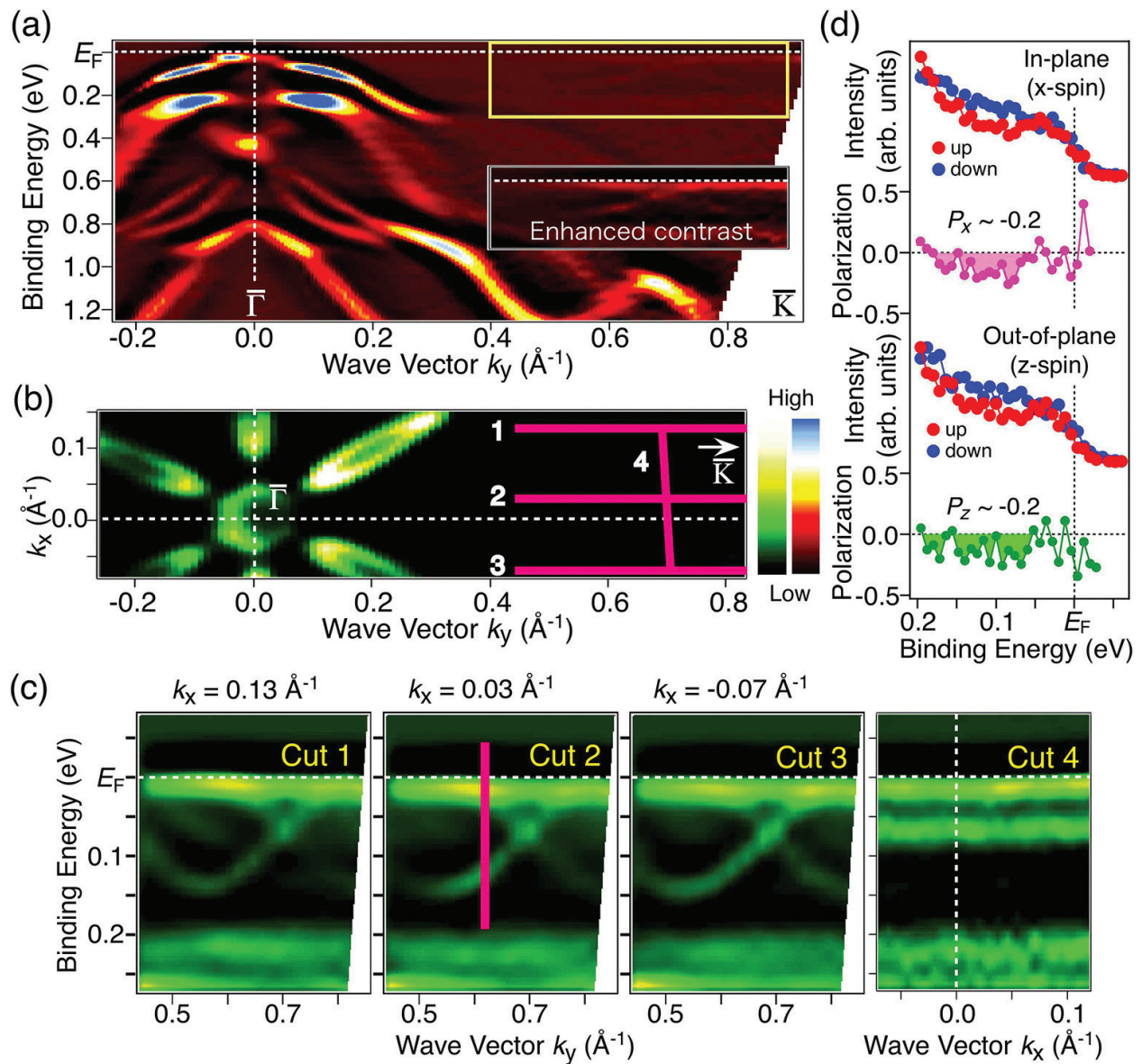


Figure 15. (a) Band structure of a Bi thin film along the $\bar{\Gamma}$ \bar{K} high-symmetry lines. To better trace the weak signal around the \bar{K} points, an enhanced color scale image is shown in the inset. (b) ARPES intensity plot at E_F around the $\bar{\Gamma}$ \bar{K} line. (c) Band dispersion near E_F along cuts 1–4 in (b), respectively. (d) Spin-resolved EDCs for the in-plane and out-of-plane spin components at the k point indicated by the pink line in (c), together with the corresponding energy dependence of the spin polarization.

the high-symmetry point $\bar{\Gamma}$ now becomes the time-reversal-invariant momentum and is located exactly at the horizontal projection of the \bar{M} point ($k_y = 0.69 \text{ \AA}^{-1}$), which actually coincides with the intersection of the x -shaped band. **Figure 16c** displays the calculated band dispersion along the $\bar{\Gamma}$ \bar{Y} direction of Bi thin film for $d = 10$ BL. We identify two prominent dispersive bands, which cross E_F and have the edge-state origin. Moreover, the edge bands show the Rashba spin splitting due to the strong spin-orbit coupling at the edge, as evidenced by the degeneracy at the \bar{Y} point. We found that the overall spin-vector direction in the experiment, that is, sign of spin polarization for each component, is also consistent with the

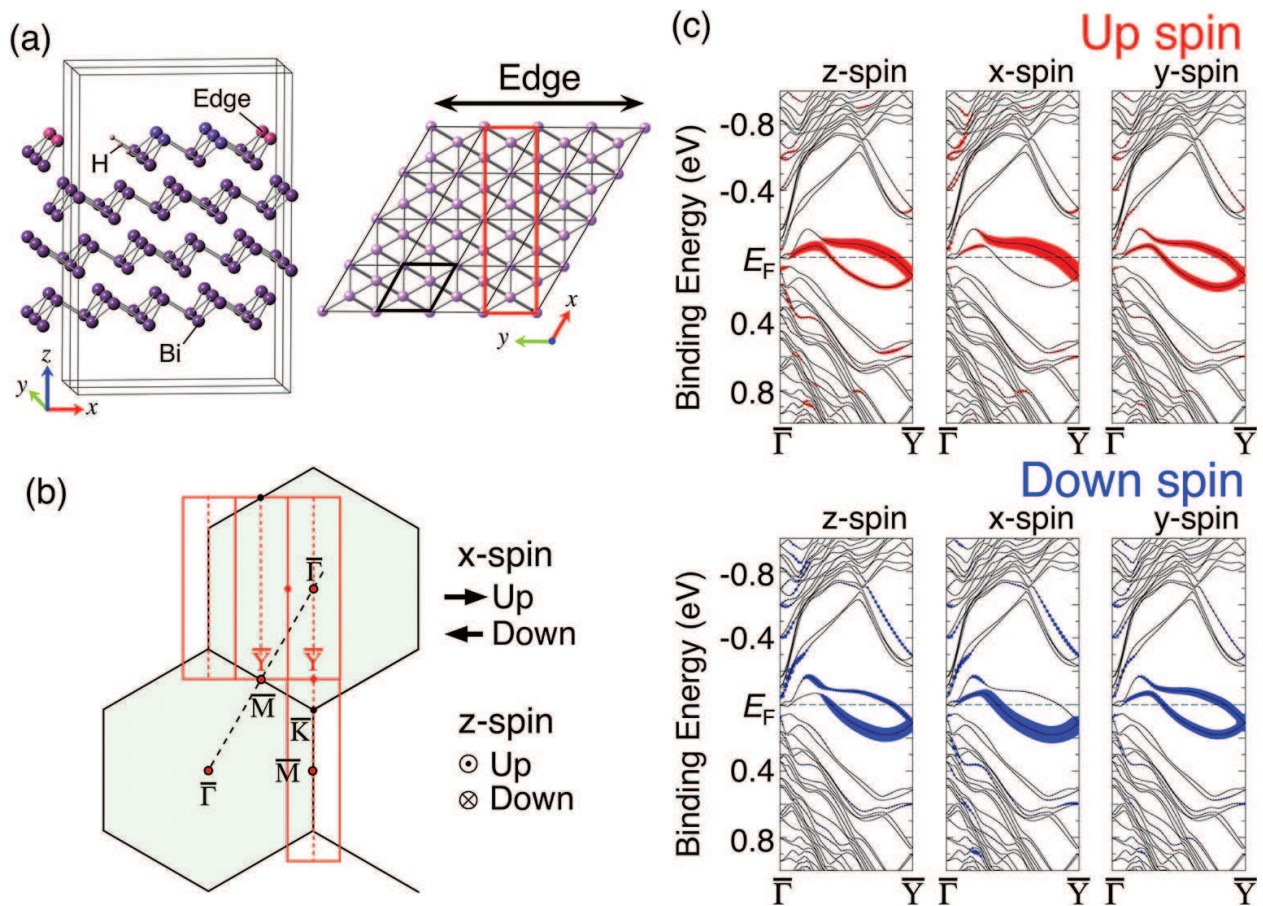


Figure 16. (a) Side and top views of the artificially constructed model crystal structure used to calculate the energy band structure of the edge state. Area enclosed by gray and red solid lines shows the unit cell. Crystal structure in the unit cell contains 1 BL Bi ribbon on 3 BL Bi where hydrogen atoms terminate one side of the edge in Bi ribbon. (b) The 1D Brillouin zone (red line) of the model crystal structure shown in (a), compared to the 2D hexagonal surface Brillouin zone (black line). (c) Band calculations for the model crystal structure along the $\bar{\Gamma}$ - \bar{Y} line. The wide of red or blue curves indicates the concentration of the up- and down-spin electrons along the axis specified in the figure.

calculation, while the absolute magnitude of the spin polarization in the experiment (~ 0.2) is much smaller than that of the calculation (~ 0.26 to 0.64) in both the in-plane and out-of-plane components, likely due to a finite contribution from the angle-integrated-type background in the ARPES spectra and the spin-orbit entanglement effect [41]. Finally, we have estimated the Rashba parameter α_r by numerical simulation for the 1D parabolic band with the SOC and obtained $\alpha_r = 0.80 \pm 0.05 \text{ eV\AA}$ (Figure 17). This value is much larger than that for the 2D surface state (0.56 eV\AA) [11, 15], and the difference could be explained in terms of the presence of an in-plane potential gradient [15, 42] at the edge in addition to the out-of-plane component, which already exists in the 2D film, as supported by observation of the out-of-plane spin polarization as large as the in-plane counterpart. Recently, STM study on the edge states of Bi crystal and thin film [43, 44]. The STM study reported that one of two types of edges, where Bi atoms are terminated at close to vacuum, which corresponds to our calculation, has a 1D character. The band dispersion of the edge state observed in ARPES shows a good agreement with the calculated bands, suggesting that both ARPES and STM observe the same edge state. It is true that 1D electronic state that observed our ARPES measurement is localized at edge.

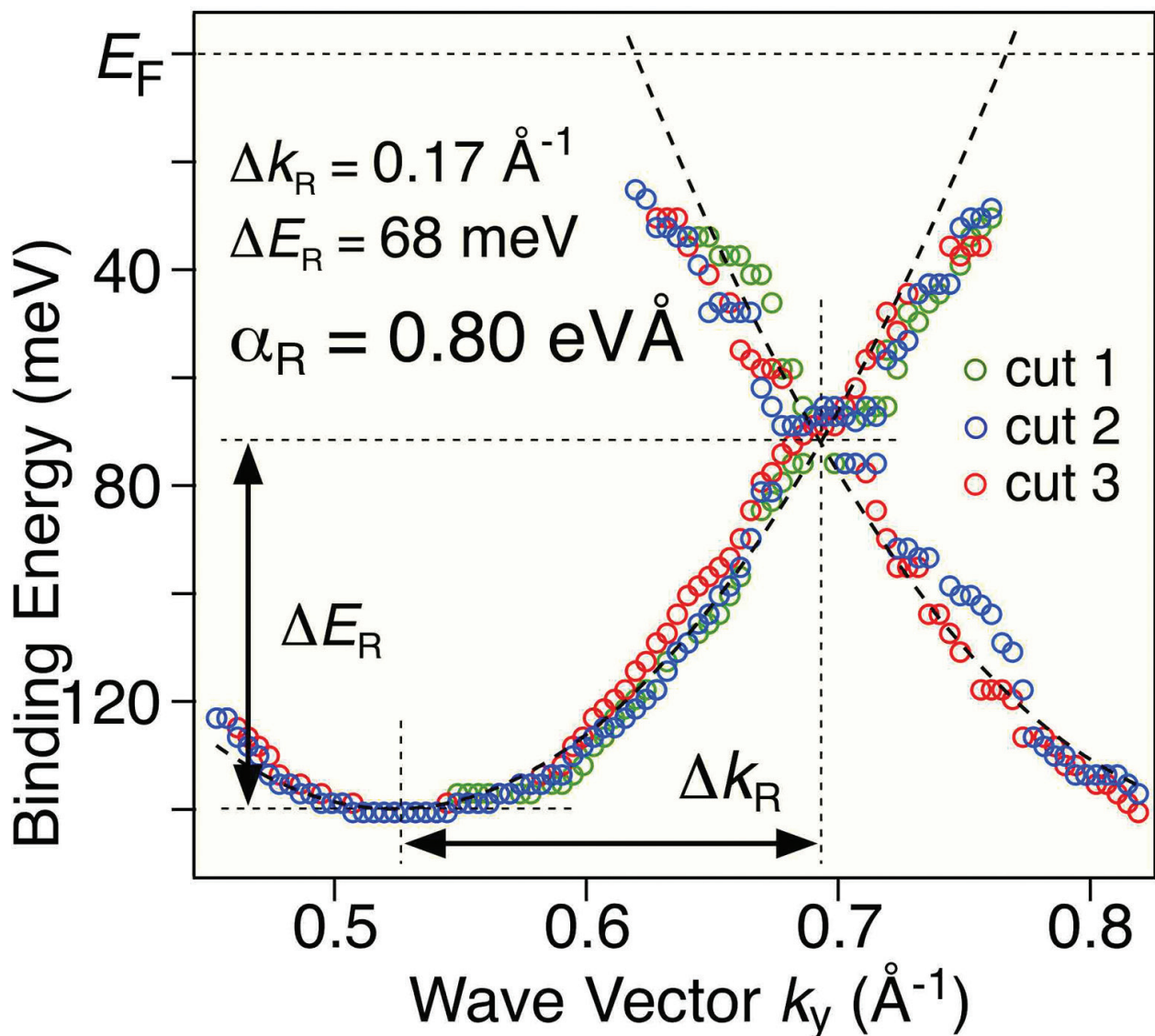


Figure 17. Experimental band dispersion for cuts 1–3 extracted from the peak position of the EDCs in Figure 15c, compared with the numerical simulation for a simple 1D Rashba splitting (dashed black curve).

The edge state in Bi would be also useful in realizing novel physical properties and new spintronic devices.

4. Conclusions

We have demonstrated anomalous Rashba effect of Bi thin film on Si(1 1 1) by using spin-resolved ARPES. Major findings of the present work are the following three features: (i) the surface Rashba states of Bi exhibit the asymmetric in-plane spin polarization and the giant out-of-plane spin polarization, (ii) the spin polarization of the surface states is reduced on decreasing thickness and (iii) 1D band dispersion from the edge state of Bi islands on Si(1 1 1) exhibits large Rashba effect. These observed peculiar spin states are not explained in terms of

the conventional Rashba effect, and these results open a pathway for realizing exotic physical properties at the strong SOC systems.

Acknowledgements

This study is a collaborative research with Prof. Takahashi, Associate Prof. Sato and Associate Prof. Souma in Tohoku University and Prof. Oguchi in Osaka University. We thank K. Sugawara and K. Kosaka for his assistance in the ARPES experiment. This work was supported by JSPS, MEXT of Japan and the Mitsubishi foundation.

Author details

Akari Takayama

Address all correspondence to: a.takayama@surface.phys.s.u-tokyo.ac.jp

The University of Tokyo, Tokyo, Japan

References

- [1] Baibich MN, Broto JM, Fert A, Nguyen Van Dau F, Petroff F, Eitenne P, Creuzet G, Friedrich A, and Chazelas J. Giant magnetoresistance of (001)Fe/(001)Cr magnetic superlattices. *Phys. Rev. Lett.* 1988;**61**:2472. doi:10.1103/PhysRevLett.61.2472
- [2] Awschalom D and Samarth N. Trend: Spintronics without magnetism. *Physics* 2009;**2**:50. doi:10.1103/Physics.2.50
- [3] Datta S and Das B. Electronic analog of the electro-optic modulator. *Appl. Phys. Lett.* 1990;**56**:665–667. DOI:10.1063/1.102730
- [4] Bychkov YA and Rashba EI. Properties of a 2D electron gas with lifted spectral degeneracy. *JETP Lett.* 1984;**39**:78–81.
- [5] Hasan MZ and Kane CL. Colloquium: topological insulators. *Rev. Mod. Phys.* 2010;**82**:3045. doi:10.1103/RevModPhys.82.3045
- [6] Qi XL and Zhang SC. Topological insulators and superconductors. *Rev. Mod. Phys.* 2011;**83**:1057. doi:10.1103/RevModPhys.83.1057
- [7] LaShell S, McDougall BA, and Jensen E. Spin splitting of an Au(1 1 1) surface state band observed with angle resolved photoelectron spectroscopy. *Phys. Rev. Lett.* 1996;**77**:3419. doi:10.1103/PhysRevLett.77.3419
- [8] Hofmann P. The surfaces of bismuth: structural and electronic properties. *Prog. Surf. Sci.* 2006;**81**:191. doi:10.1016/j.progsurf.2006.03.001

- [9] Sugawara K, Sato T, Souma S, Takahashi T, Arai M, and Sasaki T. Fermi surface and anisotropic spin-orbit coupling of Sb(1 1 1) studied by angle-resolved photoemission spectroscopy. *Phys. Rev. Lett.* 2006;**96**:046411. doi:10.1103/PhysRevLett.96.046411
- [10] Ast CR and Höchst H. Fermi surface of Bi(1 1 1) measured by photoemission spectroscopy. *Phys. Rev. Lett.* 2001;**87**:177602. doi:10.1103/PhysRevLett.87.177602
- [11] Koroteev YM, Bihlmayer G, Gayone JE, Chulkov EV, Blügel S, Echenique PM, and Hofmann PH. Strong spin-orbit splitting on Bi surfaces. *Phys. Rev. Lett.* 2004;**93**:046403. doi:10.1103/PhysRevLett.93.046403
- [12] Hirahara T, Nagao T, Matsuda I, Bihlmayer G, Chulkov EV, Koroteev YM, Echenique PM, Saito M, and Hasegawa S. Role of spin-orbit coupling and hybridization effects in the electronic structure of ultrathin Bi films. *Phys. Rev. Lett.* 2006;**97**:146803. doi:10.1103/PhysRevLett.97.146803
- [13] Hirahara T, Miyamoto K, Matsuda I, Kadono T, Kimura A, Nagao T, Bihlmayer G, Chulkov EV, Qiao S, Shimada K, Namatame H, Taniguchi M, and Hasegawa S. Direct observation of spin splitting in bismuth surface states. *Phys. Rev. B* 2007;**76**:153305. doi:10.1103/PhysRevB.76.153305
- [14] Kimura A, Krasovskii EE, Nishimura R, Miyamoto K, Kadono T, Kanomaru K, Chulkov EV, Bihlmayer G, Shimada K, Namatame H, and Taniguchi M. Strong Rashba-type spin polarization of the photocurrent from bulk continuum states: experiment and theory for Bi(1 1 1). *Phys. Rev. Lett.* 2010;**105**:076804. doi:10.1103/PhysRevLett.105.076804
- [15] Ast CR, Henk J, Ernst A, Moreschini L, Falub MC, Pacilé D, Bruno P, Kern K, and Grioni M. Giant spin splitting through surface alloying. *Phys. Rev. Lett.* 2007;**98**:186807. doi:10.1103/PhysRevLett.98.186807
- [16] Meier F, Dil H, Checa JL, Patthey L, and Osterwalder J. Quantitative vectorial spin analysis in angle-resolved photoemission: Bi/Ag(1 1 1) and Pb/Ag(1 1 1). *Phys. Rev. B.* 2008;**77**:165431. doi:10.1103/PhysRevB.77.165431
- [17] Gierz I, Suzuki T, Frantzeskakis E, Pons S, Ostanin S, Ernst A, Henk J, Grioni M, Kern K, and Ast CR. Silicon surface with giant spin splitting. *Phys. Rev. Lett.* 2009;**103**:046803. doi:10.1103/PhysRevLett.103.046803
- [18] Sakamoto K, Kakuta H, Sugawara K, Miyamoto K, Kimura A, Kuzumaki T, Ueno N, Annese E, Fujii J, Kodama A, Shishidou T, Namatame H, Taniguchi M, Sato T, Takahashi T, and Oguchi T. Peculiar Rashba splitting originating from the two-dimensional symmetry of the surface. *Phys. Rev. Lett.* 2009;**103**:156801. doi:10.1103/PhysRevLett.103.156801
- [19] Frantzeskakis E, Pons S, and Grioni M. Band structure scenario for the giant spin-orbit splitting observed at the Bi/Si(1 1 1) interface Emmanouil. *Phys. Rev. B* 2010;**82**:085440. doi:10.1103/PhysRevB.82.085440
- [20] Sakamoto K, Oda T, Kimura A, Miyamoto K, Tsujikawa M, Imai A, Ueno N, Namatame H, Taniguchi M, Eriksson PEJ, and Uhrberg RIG. Abrupt rotation of the Rashba spin to

- the direction perpendicular to the surface. *Phys. Rev. Lett.* 2009;**102**:096805. doi:10.1103/PhysRevLett.102.096805
- [21] Yaji K, Ohtsubo Y, Hatta S, Okuyama H, Miyamoto K, Okuda T, Kimura A, Namatame T, Taniguchi M, and Aruga T. Large Rashba spin splitting of a metallic surface-state band on a semiconductor surface. *Nature Commun.* 2010;**1**:17. doi:10.1038/ncomms1016
- [22] Matetskiy AV, Ichinokura S, Bondarenko LV, Tupchaya AY, Gruznev DV, Zotov AV, Saranin AA, Hobara R, Takayama A, and Hasegawa S. Two-dimensional superconductor with a giant Rashba Effect: one-atom-layer Tl-Pb compound on Si(1 1 1). *Phys. Rev. Lett.* 2015;**115**:147003. doi:10.1103/PhysRevLett.115.147003
- [23] Barke I, Zheng F, Rughheimer TK, and Himpsel FJ. Experimental evidence for spin-split bands in a one-dimensional chain structure. *Phys. Rev. Lett.* 2006;**97**:226405. doi:10.1103/PhysRevLett.97.226405.
- [24] Wells JW, Dil JH, Meier F, Lobo-Checa J, Petrov VN, Osterwalder J, Ugeda MM, Fernandez-Torrente I, Pascual JI, Rienks EDL, Jensen MF, and Hofmann Ph. Nondegenerate metallic states on Bi(1 1 4): a one-dimensional topological metal. *Phys. Rev. Lett.* 2009;**102**:096802. doi:10.1103/PhysRevLett.102.096802
- [25] Quay CHL, Hughes TL, Sulpizio JL, Pfeiffer LN, Baldwin KW, West KW, Goldhaber-Gordon D, and de Picciotto R. Observation of a one-dimensional spin-orbit gap in a quantum wire. *Nat. Phys.* 2010;**6**:336. doi:10.1038/nphys1626
- [26] Pershin YV, Nesteroff JA, and Privman V. Effect of spin-orbit interaction and in-plane magnetic field on the conductance of a quasi-one-dimensional system. *Phys. Rev. B.* 2004;**69**:121306(R). doi:10.1103/PhysRevB.69.121306
- [27] Takayama A, Sato T, Souma S, and Takahashi T. Giant out-of-plane spin component and the asymmetry of spin polarization in surface Rashba States of Bismuth thin film. *Phys. Rev. Lett.* 2011;**106**:166401. doi:10.1103/PhysRevLett.106.166401
- [28] Takayama A, Sato T, Souma S, Oguchi T, and Takahashi T. Tunable spin polarization in bismuth ultrathin film on Si(1 1 1). *Nano Lett.* 2012;**12**:1776. doi:10.1021/nl2035018
- [29] Takayama A, Sato T, Souma S, Oguchi T, and Takahashi T. One-dimensional edge states with giant spin splitting in a bismuth thin film. *Phys. Rev. Lett.* 2015;**114**:066402. doi:10.1103/PhysRevLett.114.066402
- [30] Souma S, Takayama A, Sugawara K, Sato T, and Takahashi T. Ultrahigh-resolution spin-resolved photoemission spectrometer with a mini Mott detector. *Rev. Sci. Instrum.* 2010;**81**:095101. doi:10.1063/1.3480542
- [31] Schlier E and Farnsworth HE. Structure and adsorption characteristics of clean surfaces of germanium and silicon. *J. Chem. Phys.* 1959;**30**:917. doi:10.1063/1.1730126
- [32] Takayanagi K, Tanishiro Y, Takahashi M, and Takahashi S. Structural analysis of Si(1 1 1)-7×7 by UHV-transmission electron diffraction and microscopy. *J. Vac. Sci. Technol. A.* 1985;**3**:1502. doi:10.1116/1.573160

- [33] Viernow J, Lin JL, Petrovykh DY, Leibsle FM, Men FK, and Himpsel FJ. Regular step arrays on silicon. *Appl. Phys. Lett.* 1998;**72**:948. doi:10.1063/1.120882
- [34] Nagao T, Sadowski JT, Saito M, Yaginuma S, Fujikawa Y, Kogure T, Ohno T, Hasegawa Y, Hasegawa S, and Sakurai T. Nanofilm allotrope and phase transformation of ultrathin Bi film on Si(1 1 1)-7×7. *Phys. Rev. Lett.* 2004;**93**:105501. doi:10.1103/PhysRevLett.93.105501
- [35] Kirschner J, Feder R, and Wendelken JF. Electron spin polarization in energy- and angle-resolved photoemission from W(0 0 1): experiment and theory. *Phys. Rev. Lett.* 1981;**47**:614. doi:10.1103/PhysRevLett.47.614
- [36] Oepen HP, Hunlich K, and Kirschner J. Spin-dependent photoemission intensities from solids. *Phys. Rev. Lett.* 1986;**56**:496. doi:10.1103/PhysRevLett.56.496
- [37] Zhang HJ, Liu CX, Qi XL, Deng XY, Dai X, Zhang SC, and Fang Z. Electronic structures and surface states of the topological insulator $\text{Bi}_{1-x}\text{Sb}_x$. *Phys. Rev. B.* 2009;**80**:085307. doi:10.1103/PhysRevB.80.085307
- [38] Fu L. Hexagonal warping effects in the surface states of the topological insulator Bi_2Te_3 . *Phys. Rev. Lett.* 2009;**103**:266801. doi:10.1103/PhysRevLett.103.266801
- [39] Souma S, Kosaka K, Sato T, Komatsu M, Takayama A, Takahashi T, Kriener M, Segawa K, and Ando Y. Direct measurement of the out-of-plane spin texture in the dirac-cone surface state of a topological insulator. *Phys. Rev. Lett.* 2011;**106**:216803. doi:10.1103/PhysRevLett.106.216803
- [40] Zhang Y, He K, Chang CZ, Song CL, Wang LL, Chen X, Jia JF, Fang Z, Dai X, Shan WY, Shen SQ, Niu Q, Qi XL, Zhang SC, Ma XC, and Xue QK. Crossover of the three-dimensional topological insulator Bi_2Se_3 to the two-dimensional limit. *Nat. Phys.* 2010;**6**:584. doi:10.1038/nphys1689
- [41] Yazyev OV, Moore JE, and Louie SG. Spin polarization and transport of surface states in the topological insulators Bi_2Se_3 and Bi_2Te_3 from first principles. *Phys. Rev. Lett.* 2010;**105**:266806. doi:10.1103/PhysRevLett.105.266806
- [42] Park J, Jung S, Jung MC, Yamane H, Kosugi N, and Yeom H. Self-assembled nanowires with giant Rashba split bands. *Phys. Rev. Lett.* 2013;**110**:036801. doi:10.1103/PhysRevLett.110.036801
- [43] Drozdov IK, Alexandradinata A, Jeon S, Nadj-Perge S, Ji H, Cava RJ, Andrei Bernevig B, and Yazdani A. One-dimensional topological edge states of bismuth bilayers. *Nat. Phys.* 2014;**10**:664. doi:10.1038/nphys3048
- [44] Kawakami N, Lin CL, Kawai M, Arafune R, and Takagi N. One-dimensional edge state of Bi thin film grown on Si(1 1 1). *Appl. Phys. Lett.* 2015;**107**:031602. doi:10.1063/1.4927206

